NUMERICAL EVALUATION OF MAGNETIC COORDINATES FOR PARTICLE-TRANSPORT STUDIES IN ASYMMETRIC PLASMAS

BY

Kuo-Petravic and Allen H. Boozer

January 1982

PLASMA PHYSICS LABORATORY

PRINCETON UNIVERSITY
PRINCETON, NEW JERSEY

PREPARED FOR THE U.S. DEPARTMENT OF ENERGY,
UNDER CONTRACT DE-AC02-76-CHO-3073.

PPPL--1866

DE82 010673

Numerical Evaluation of Magnetic Coordinates for Particle Transport Studies in Asymmetric Plasmas

by

Gioietta Kuo-Petravic and Allen H. Boozer

Plasma Physics Laboratory, Princeton University

Princeton, New Jersey 08544

MAGNETIC CO-ORDS FOR ASYMMETRIC PLASMAS

Send Proofs to:

G. Kuo-Petravic

Theory Division

Plasma Physics Laboratory

Princeton University

Princeton, New Jersey 08544

ABSTRACT

We describe here a numerical procedure for the evaluation of magnetic coordinates given a toroidal, scalar pressure plasma with an arbitrary magnetic field. The accurate representation of magnetic field strength in this way is invaluable for the calculation of drift orbits and transport in asymmetric plasmas. We include here an example of how the results are combined with the guiding center drift equations to calculate diffusion coefficients in a Tokatron plasma.

Introduction

Particle transport in thermonuclear plasmas depend basically on the number of directions of symmetry in the plasma configuration. The search for alternative toroidal confinement devices to the Tokamak has led to systems like the stellarator, Tokatron ... etc., all with less symmetry and consequently enhanced diffusion especially at low collisionality regimes. Even for the Tokamak, assymetry effects are important for it is well known that a Tokamak ripple of 1% or less is able to significantly enhance the ion loss. Therefore, any numerical technique enabling us to understand asymmetric plasmas would be most welcome. Deficiencies in our tools have long been recognized. Not only are the equilibrium and stability properties difficult to simulate, even the single particle confinement characteristics are largely unknown. In these asymmetric configurations coordinates based on the magnetic field lines become the natural coordinates to use. In this system, the rapid motion of particles parallel to the field line is well separated from the slow drift motion and the electric potential is normally uniform on a coordinate surface. The usefulness of magnetic coordinates has long been recognized in plasma equilibrium and stability studies.[1,2,3] Recently it was shown[4,5,6] that the guiding center drift equations are particularly simple in magnetic coordinates involving only a knowledge of the scalar quality B, the magnetic field strength, and its derivatives. From this it follows that particle transport, with and without collisions, may be readily computed with a high degree of accuracy in a minimum of computer time.

However, the correspondence between the magnetic coordinates and the Cartesian system remains a difficult problem. In this paper we describe the realization of a technique[7] whereby the magnetic field strength is computed in magnetic coordinates by Fourier decomposition for a toroidal plasma with

scalar pressure equilibrium and closed magnetic surfaces. This procedure assumes a knowledge of the magnetic field $B(R,Z,\Phi)$ at all points in the torus, where R, Z, and Φ are the cylindrical coordinates. This field can be derived from a combination of external current filaments and plasma currents assuming that the plasma equilibrium is known.

We also show how the results of this decomposition may be coupled to the guiding center drift equations in our Monte-Carlo code[6] to obtain particle transport coefficients.

The Magnetic Coordinates and Their Derivation

The use of magnetic coordinates (ψ, θ_o, χ) can best be illustrated by deriving the simple guiding center drift equations in a general field $\vec{B}$ in these coordinates. The guiding center velocity $\vec{v}$ can be written:

$$\vec{v} = \frac{v_\parallel}{B} [\vec{B} + \vec{\nabla} \times \rho_\parallel \vec{B}] \qquad \text{where} \qquad \rho_\parallel = \frac{v_\parallel}{\omega_c} \quad . \tag{1}$$

We need simple convariant and contravariant representations for $\vec{B}$. In a scalar pressure equilibrium

$$\vec{\nabla} p = \frac{1}{c} \vec{j} \times \vec{B}, \quad ,$$

the appropriate coordinates are

$$\psi, \ \theta_o, \ \chi \qquad \text{with} \ \vec{B} = \nabla\psi \times \vec{\nabla}\theta_o \qquad \text{contravariant} \tag{2}$$

$$= \nabla\chi + \beta\nabla\psi \qquad \text{covariant} \quad .$$

The drift equations are:

$$\frac{d\psi}{dt} = c\,\frac{\partial\Phi}{\partial\theta_o} + \left(\frac{c}{e}\,\mu + \frac{eB}{mc}\,\rho_{\parallel}^2\right)\frac{\partial B}{\partial\theta_o}\,,$$

$$\frac{d\theta_o}{dt} = -\,c\,\frac{\partial\Phi}{\partial\psi} - \left(\frac{c}{e}\,\mu + \frac{eB}{mc}\,\rho_{\parallel}^2\right)\frac{\partial B}{\partial\psi}\,,$$

$$\frac{d\chi}{dt} = \frac{eB^2}{mc}\,\rho_{\parallel}\,, \qquad (3)$$

$$\frac{d\rho_{\parallel}}{dt} = -\,c\,\frac{\partial\Phi}{\partial\chi} - \frac{mc}{eB}\left(\frac{c}{B}\left(\mu + \frac{eB}{mc}\,\rho_{\parallel}^2\right)\right)\frac{\partial B}{\partial\chi}$$

where (eB/mc) = ion cyclotron frequency

$$\frac{1}{2}\,mv_{\perp}^2 = \mu B$$

Φ = electrostatic potential

and

c = velocity of light .

The definition of the ψ, θ_o, χ coordinates above imply that the same $\vec{B}$ is obtained for any transformation

$$\theta_o \rightarrow \theta_o + \theta^*(\psi)\,,$$

$$\chi \rightarrow \chi + \chi^*(\psi)\,,$$

$$\beta \rightarrow \beta - \frac{d\chi^*(\psi)}{d\psi}\,. \qquad (4)$$

In a torus, poloidal and toroidal angles θ and ϕ can be defined such that

$$\chi = g(\psi)\phi + I(\psi)\theta \ ,$$

$$\theta = \theta_o + \iota(\psi)\phi \quad , \tag{5}$$

where

$\frac{c}{2}\, g(\psi)$ = the total poloidal current outside a flux surface ψ ,

$\frac{c}{2}\, I(\psi)$ = the total toroidal current inside a flux surface ψ ,

$\iota(\psi)$ = rotational transform.

The periodicities in θ and ϕ in a torus enable us to write down for any scalar function like B, the magnetic field strength

$$B(\psi,\theta,\phi) = \sum_{n,m} \{a_{nm} \exp[i(n\phi - m\phi)]\} \ . \tag{6}$$

Using (5) we obtain

$$n\phi - m\theta = \frac{n-m\iota}{g+\iota I}\ \chi - \frac{mg+nI}{g+\iota I}\ \theta_o \ . \tag{7}$$

We assume that $B(R,Z,\Phi)$ in cylindrical system is numerically known anywhere within the torus. We can integrate along a field line to obtain $B(\chi)$, where χ is the magnetic coordinate along the field line derived from (2) as

$$\chi = \int B \, d\ell \, ,$$

where $d\ell$ is a differential distance along the field line.

Since a field line must obey ψ = constant and θ_o = constant by definition throughout this integration, we can choose our initial point to be $(\psi,0,0)$. Thus Eqs. (6) and (7) are simplified:

$$B(\chi) = \sum_{n,m} \{a_{nm} \exp[i(\omega_{nm}\chi)]\}$$

$$\omega_{nm} = \frac{n-m\iota}{q+\iota I} \, . \tag{8}$$

Since $B(\chi)$ is in general not a periodic function unless ψ happens to coincide with a rational surface, the mismatch of $B(\chi)$ at $\chi = \pm\chi^*$ can give rise to spurious noise in the Fourier spectrum. Increasing χ_* only improves the spectrum linearly. However, the convergence can be made exponential by multiplying $B(\chi)$ by a Gaussian. This Gaussian should have a width much smaller than the range of integration χ_*, but much broader than the frequencies of interest in $B(\chi)$. Let $A(\omega)$ be the Fourier transform of $B(\chi)$ times a Gaussian of width χ_*/η.

$$A(\omega) \equiv \int_{-\chi_*}^{\chi_*} B(\chi)\left[\frac{\eta}{(2\pi)^{1/2}\chi_*} \exp\left(-\frac{\eta^2}{2}\frac{\chi^2}{\chi_*^2}\right)\right] \exp(-i\omega\chi) \, d\chi \, ,$$

$$= \int_{-\chi_*}^{\chi_*} F(\chi) \exp(-i\omega\chi) \, d\chi \tag{9}$$

then

$$A(\omega) = \sum_{n,m} a_{nm} \exp \{- \frac{1}{2} [(\omega_{nm} - \omega)/\omega_*]^2\}$$

where $\omega_* = \eta/\chi_*$ gives the broadening of the spectrum to be expected from a Gaussian of width χ_*/η. By adjusting the parameter η, the width of the Gaussian may be tuned to give minimum mismatch at $\chi = \pm \chi_*$ consistant with a clear separation in the Gaussian maxima of the function $A(\omega)$.

The values of a_{nm} and ω_{nm}, extracted from the Fourier spectrum, can be used in Eq. (8) to produce $B(\psi, \theta_o, \chi)$.

II Application to a Tokatron Plasma

We shall in this section illustrate the usefulness of the method by describing work on a toroidally asymmetric device called the Tokatron. The method itself is, of course, applicable to any toroidal geometries.

A schematic diagram of a Tokatron is shown in Fig. 1. The helical coils (I_h) produce both toroidal and poloidal fields hence giving a rotational trarsform even in the absence of a plasma. There is also a vertical current (I_t) on the axis producing toroidal field varying as 1/R. These also exists a uniform vertical magnetic field. We also assume that there will be some plasma current represented by the toroidal conductor (I_p).

We start the integration at an arbitrary point $B(\psi,0,0)$. The value of ψ will not be known until after the integration is completed and many toroidal circuits have been traced. We solve the equations for the field line in χ thus ensuring that we have B in equal intervals of χ :

$$\frac{dR}{d\chi} = \frac{B_R}{B^2} \quad ,$$

$$\frac{dZ}{d\chi} = \frac{B_Z}{B^2} \quad ,$$

$$\frac{d\Phi}{d\chi} = \frac{B_\Phi}{RB^2} \quad . \tag{10}$$

A fourth order Runge-Kutta integration scheme is used and at each step we save both the value of B as well as the associated R, Z, Φ. Figure 2 shows the projection of a field line onto a symmetry plane, a symmetry plane being one where a helical coil intersects the midplane. Figure 3 shows the points of intersection of six distinct field lines with a symmetry plane. The outlines of six concentric flux surfaces are readily discernable. The toroidal flux coordinate ψ is derived from the area integral

$$\psi = \frac{1}{2\pi} \int B \, dR \, dz = \int \frac{g}{R} \, dR \int dz \quad . \tag{11}$$

In cases like the outermost surface, labeled (F), of Fig. 3, data tend to appear in clusters due to the rotational transform ι being near a rational number. Clearly a longer integration will only slowly yield more significant points than those which exist already, so some interpolation is necessary. To perform the area integral of Eq. (11) we therefore first find a weighted least squares polynomial approximation in Chebyshev series form to the data points. Depending on the number and the configuration of the data points it may be necessary to choose a polynomial of high degree. Figure 4 shows a polynomial of 10th degree and the data points. The area integral is then simply obtained from the polynomial. Since the Tokatron has up down symmetry, it is only necessary to calculate the flux integral using one half of the flux surface only. However, since we possess independent data for the two halves, we integrate the areas for $Z > 0$ and $Z < 0$ seprately. In general the

derivation between the two values is < 0.5%.

Figure 5 shows the result of attempting to trace a flux surface inside surface labeled (A). Island formation is already in evidence; beyond this the surfaces become ergodic. Outside the surface labeled, (F), there are no good magnetic surfaces.

A judicious choice of the values for the parameters χ, η, $\Delta\chi$, N, where $\Delta\chi$ is the step length of integration and N the total number of data points, will aide in much savings for both computer time and computer storage. As can be seen from Eq. (4), the smallest distance between peaks in the Fourier spectrum is approximately ι/g if $\iota < 1$ and $I \ll g$, therefore in regimes where the rotational transform is large, peak broadening by the Gaussian is not important and η can be made large to save integration time. However, in other regimes it would be reasonable to allow the gaussian broadening to be no greater than, say, twice the intrinsic resolution of the Fourier transform process which is given by $2\pi/2\chi_*$, we have, therefore, $\omega_* = \pi/\chi_* = 2(\pi/\chi_*)$ and $\eta = 2\pi$. The smallest frequency difference $\Delta\omega$ which we wish to resolve is either ι/g or $1/g$ whichever is the smaller. Suppose we require that this $\Delta\omega$ be a few times, say η times, the line width, then $\Delta\omega = \eta\,\omega_* = \eta^2/\chi_*$ and $\chi_* = \eta^2/\Delta\omega$. Taking $\Delta\omega = \iota/g$ and $\chi = g\phi$ it may be seen that we need to follow the field line for 5 to 10 toroidal or poloidal circuits in order to have distinct peak separation. One last choice available to us lies in $\chi_* = N\Delta\chi$. Since we are often interested in only the very low frequency end of the Fourier spectrum, it is useful to minimize N and correspondingly increase $\Delta\chi$ so as to save integration time. However, $\Delta\chi$ must be kept sufficiently small to accurately follow the field lines.

Figure 6 shows $B(\chi)$ versus χ for approximately twelve poloidal circuits. In Fig. 7 we see the function $F(\chi)$ of Eq. (9) consisting

of $B(\chi)$ multiplied by a gaussian of Eq. (9). The portions of the curve at $\chi < 0$ and $\chi > 0$ have been interchanged. Since the Fast Fourier Transform package assumes that $\chi = 0$ at the leftmost point of the graph, $F(\chi)$ will now contain mostly cos $\omega\chi$ in its frequency spectrum ensuring that the output spectrum will be predominantly real and the coefficient $b_{nm} \approx 0$. From Fig. 7 it may be seen that another 20% of computer time may be saved by filling regions in the far wings of the gaussian with zeros. The precise extent of savings will depend on the structure of $B(\chi)$ and the width of the Gaussian, η, chosen.

We have used a Fast Fourier transform package named RCFFTZ which is fully vectorized and is resident on the CRAY machine at MFECC, Livermore. For 2^{14} data points our timing gave 16 msecs.

The Fourier spectrum as described by Eq. (9) is shown in Fig. 8. As expected the imaginary components b_{nm} are all $\lesssim 10^{-5}\ a_{nm}$ in the region of interest in ω. Since, in most cases, the currents are predominently poloidal, that is $I << g$, it is convenient to plot a_{nm} against $(n-m\iota)$ rather than ω_{nm} for peaks with $m = 0$ appear then as integers on the absissa. The separations between peaks with common n also give us a good method of estimating the average transform ι. Values of these coefficients can be obtained by these means to within an order of accuracy of $\sim 10^{-3}$. Taking only the eight largest components: $n = 0$, $m = 0, -1, -2, -3$ and $n = 5$, $m = 0, 1, 2, 3$ of which all have peak heights greater than 1% of a_{oo}, the DC component, we can compare the Fourier synthesized B with the original field. Fig. 9 shows this comparison.

We now have a numerical form for B in magnetic coordinates. The guiding center drift Eq. of (3), however, require the derivatives in all these directions ψ, θ_o and χ. Only the variations of $a_{nm}(\psi)$, $g(\psi)$, $I(\psi)$, $\iota(\psi)$

with ψ need to be interpolated as those of B against θ_o and χ can now be derived analytically. Bearing in mind that these derivatives need to be referenced many times during a drift orbit calculation, the speed of performance is important. We therefore chose cubic minimax polynomial fits to all the parameters which vary with ψ. Fig. 10 shows an example of this fit. The drift orbits are then advanced using the Fourier components for $B(\psi, \theta_o \chi)$ and the polynomials for the ψ interpolation of the coefficients. The trajectory of a particle undergoing pitch angle scattering over three collision times is described in magnetic coordinates (ψ, θ_o, χ) in Fig. 11. The general features exhibited here are qualitatively similar to collisional orbits in model stellarator fields, but the increased complexity in the field geometry means, for example, that trapping in local magnetic wells is no longer such a well defined concept. However, the confinement characteristics of each new geometry we study can now be easily deduced from analysis of the kind of results shown here.

Acknowledgment

This work was supported by U.S. Department of Energy Contract No. DE-AC02-76-CHO3073.

REFERENCES

1. M. D. KRUSKAL and R. M. KULSRUD, Phys. Fluids 1 (1958) 265.
2. S. HAMADA, Nucl. Fusion 2 (962) 23.
3. J. M. GREENE and J. L. JOHNSON, Phys. Fluids 5 (1962) 510.
4. A. H. BOOZER, Phys. Fluids 23 (1980) 904.
5. A. H. BOOZER, Phys. Fluids 24 (1981).
6. A. H. BOOZER and G. KUO-PETRAVIC, Phys. Fluids 24 (1981) 851.
7. A. H. BOOZER, Phys. Fluids (1982) to be published, Princeton Plasma Physics Laboratory Report, PPPL 1775 (1981).

Figure Captions

Fig. 1. Schematic diagram of a Tokatron. An outgrowth of a Tokamak where toroidal field coils have been replaced by helical coils.

Fig. 2. Projection of a magnetic field line onto a symmetry plane, which is one where a helical coil intersects the midplane. R and Z are the cylindrical coordinates.

Fig. 3. Intersections of six magnetic field lines with a symmetry plane. Six closed flux surfaces can be traced.

Fig. 4. Integration of flux enclosed by a magnetic surface by means of a least squares polynomial. The points are obtained by field integration and the solid line is the polynomial.

Fig. 5. Intersections of a magnetic field line with a symmetry plane. The starting point of this field line is on the inside of surface VI of Fig. 3.

Fig. 6. Magnetic field $B(\chi)$ against χ ($= \int B\, d\ell$) for about 12 poloidal circuits.

Fig. 7. Function $F(\chi)$ of Eq. (9) versus χ for the same extent in χ as in Fig. 6.

Fig. 8. Fourier spectrum for the real coefficients a_{nm} versus $(n-m\chi)$.

Fig. 9. Comparison of original $B(\chi)$ (full line) with $B(\chi)$ (dots) synthesized from the Fourier Spectrum.

Fig. 10. Variation of the rotational transform ι versus ψ. The solid line is the minimax cubic polynomial fit used by the drift equations.

Fig. 11. The trajectory of a particle undergoing pitch angle scattering over three collision times described in magnetic coordinates (ψ, θ_o, χ).

#81T0322

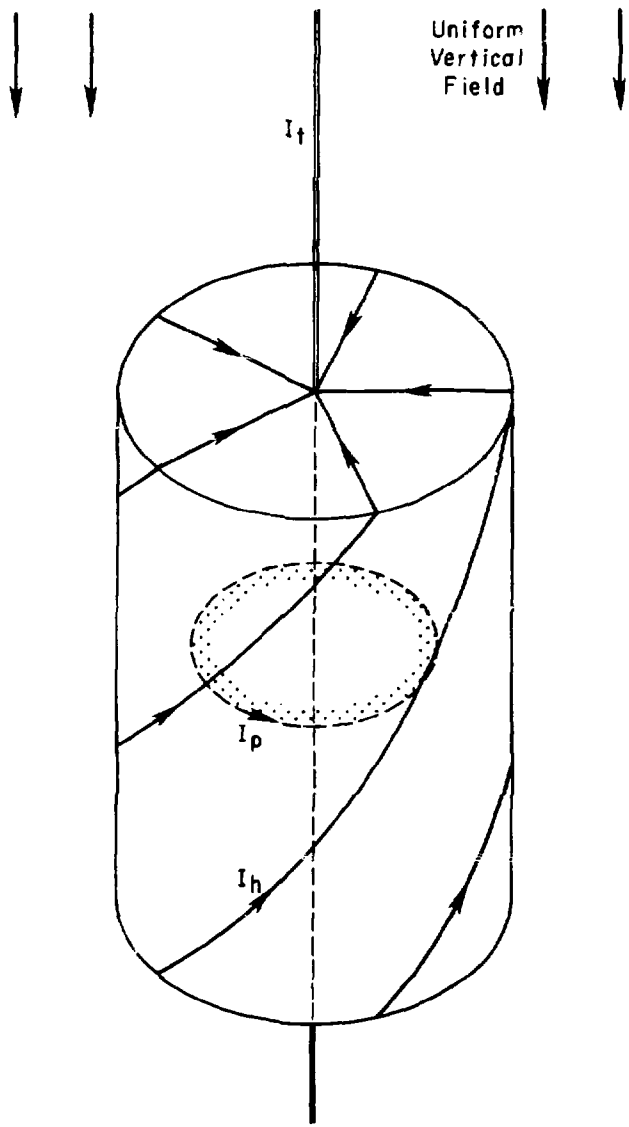

Fig. 1

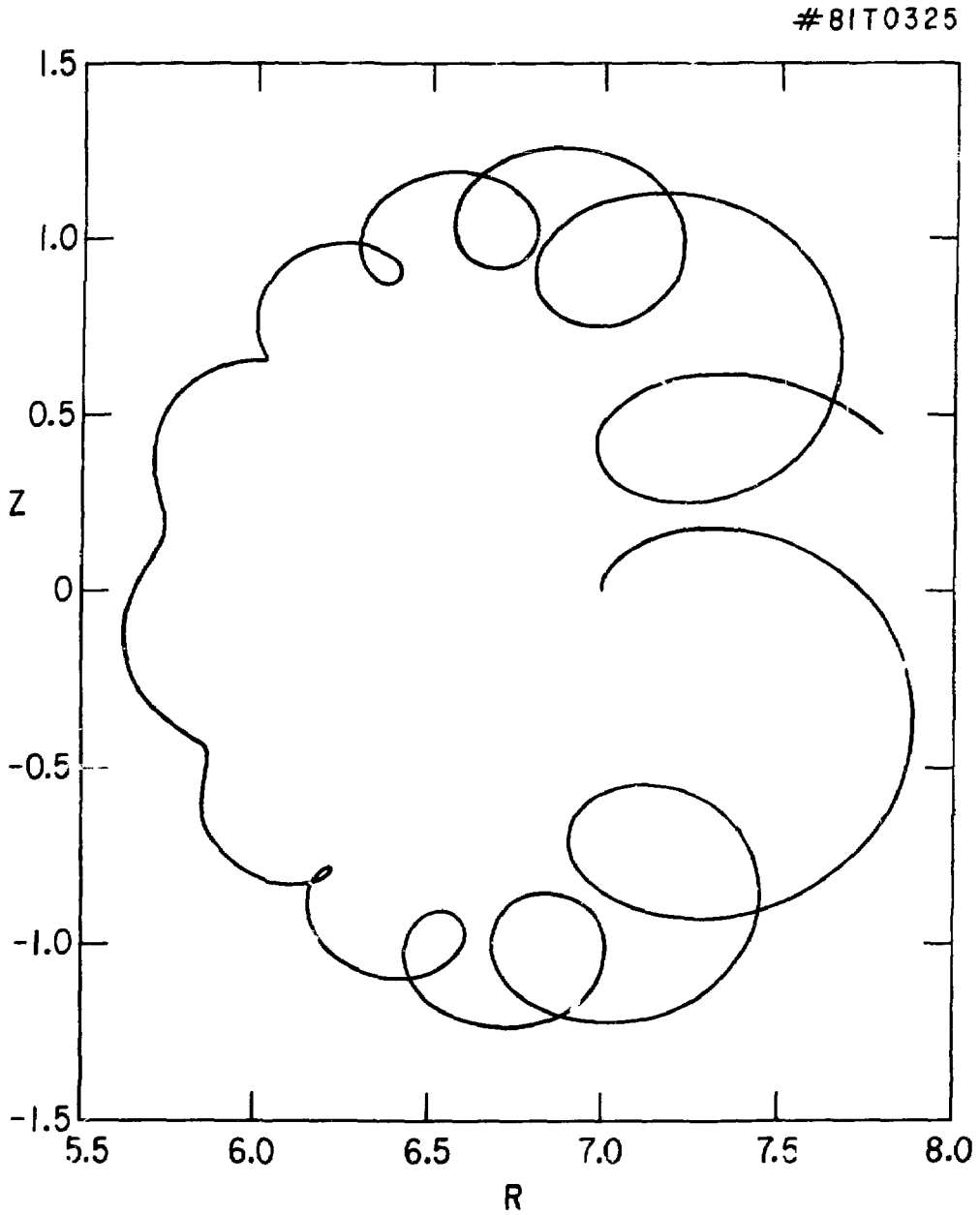

Fig. 2

#81T0334

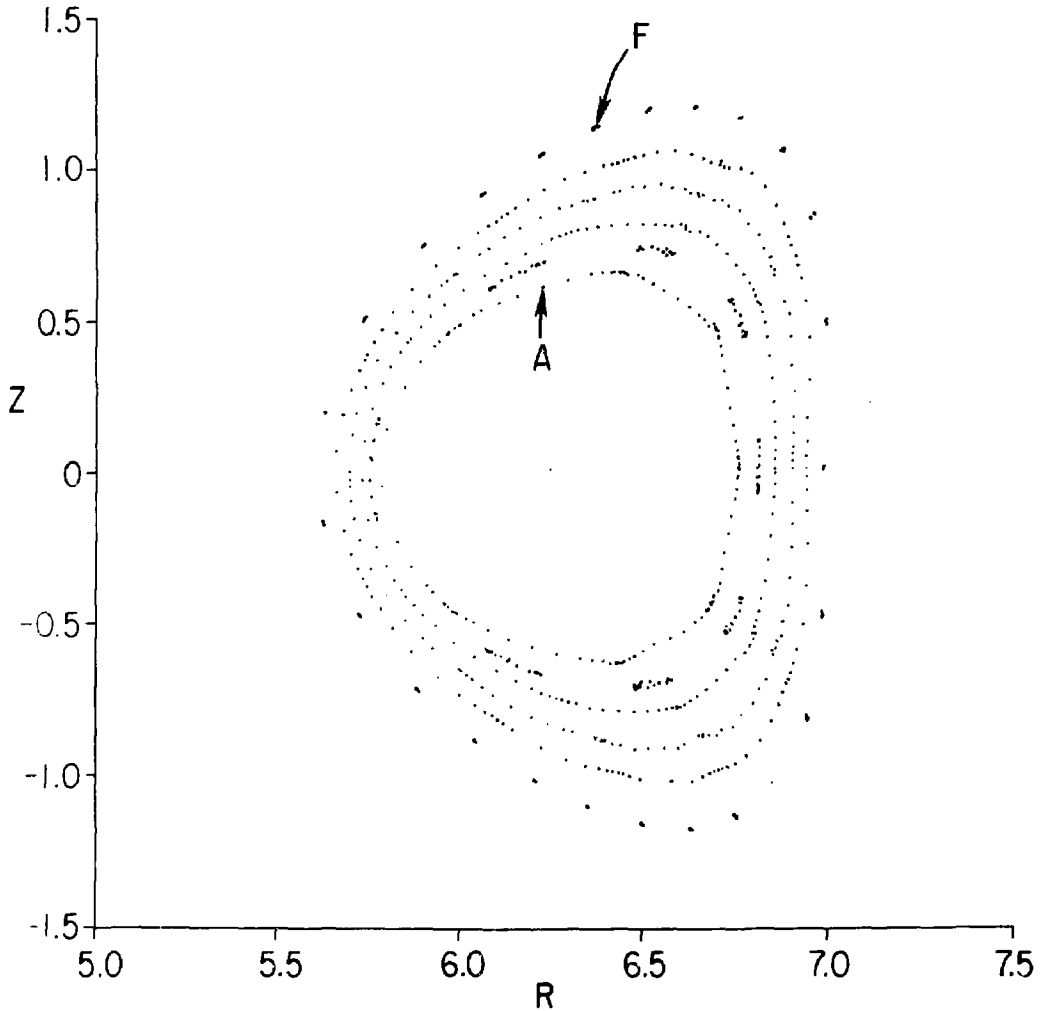

Fig. 3

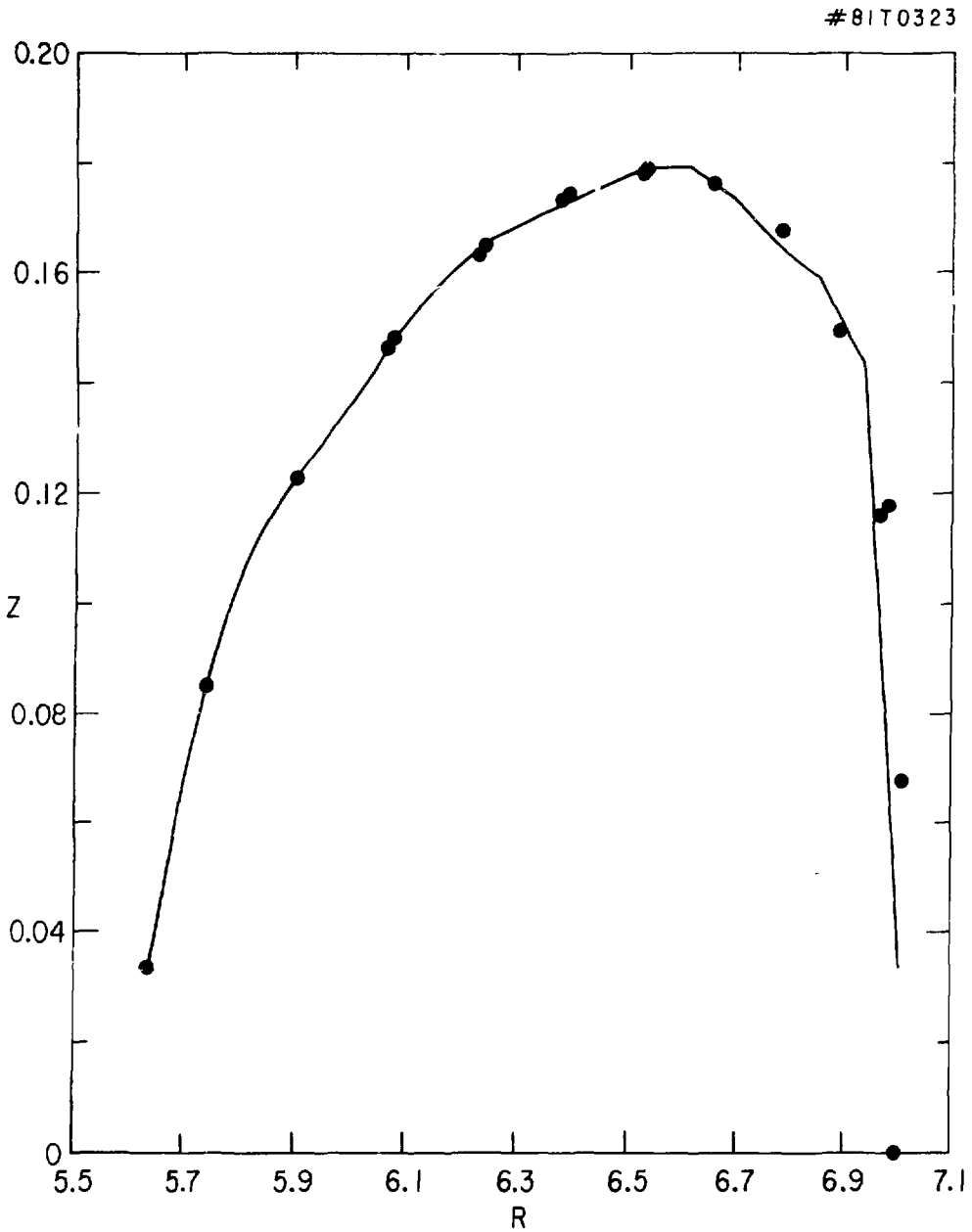

Fig. 4

#81T0333

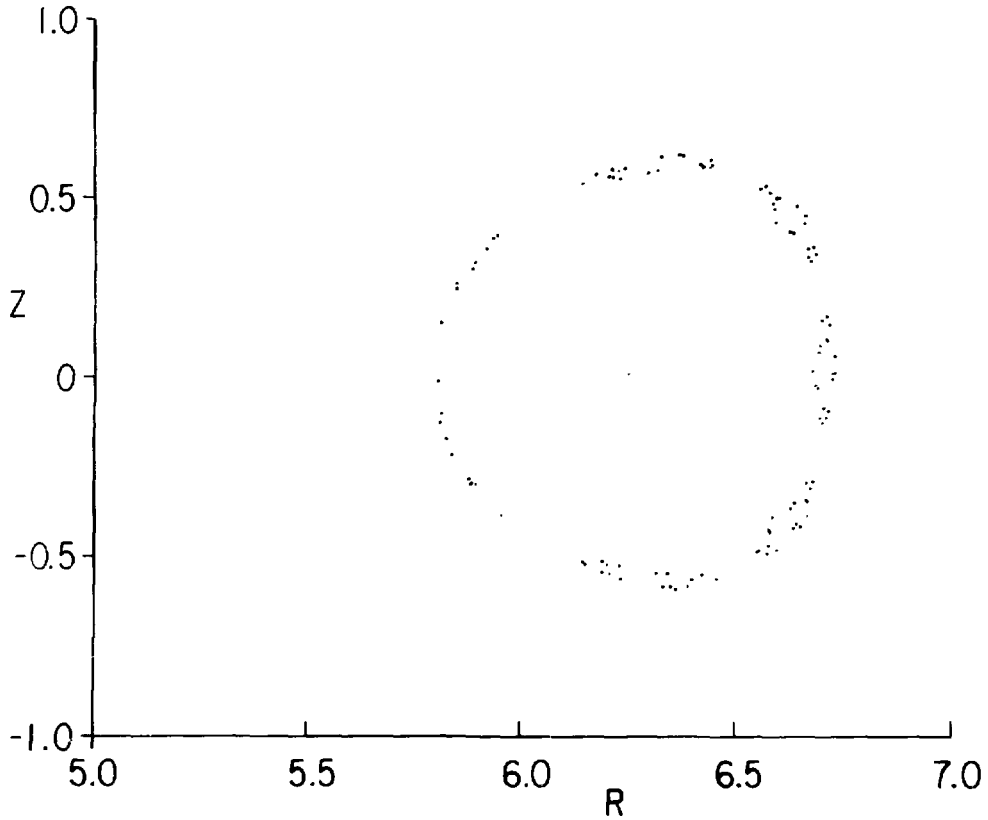

Fig. 5

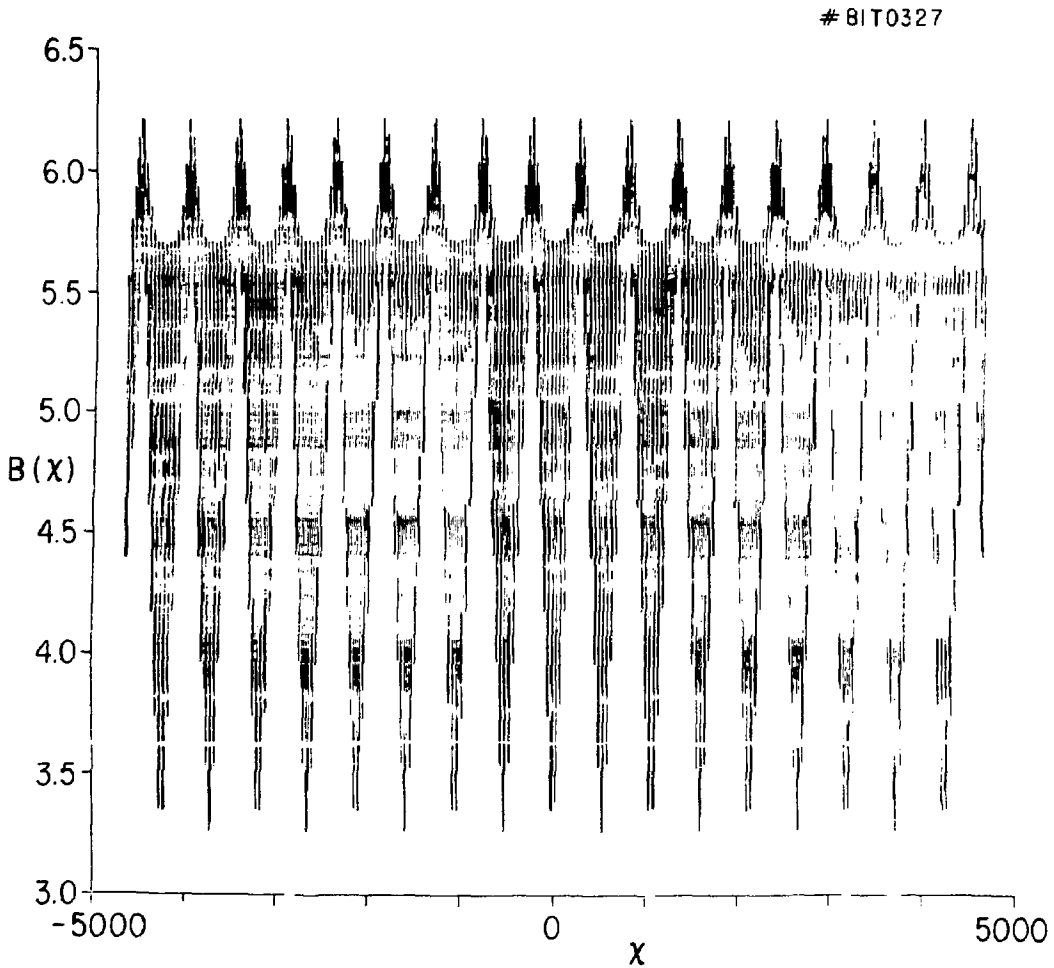

Fig. 6

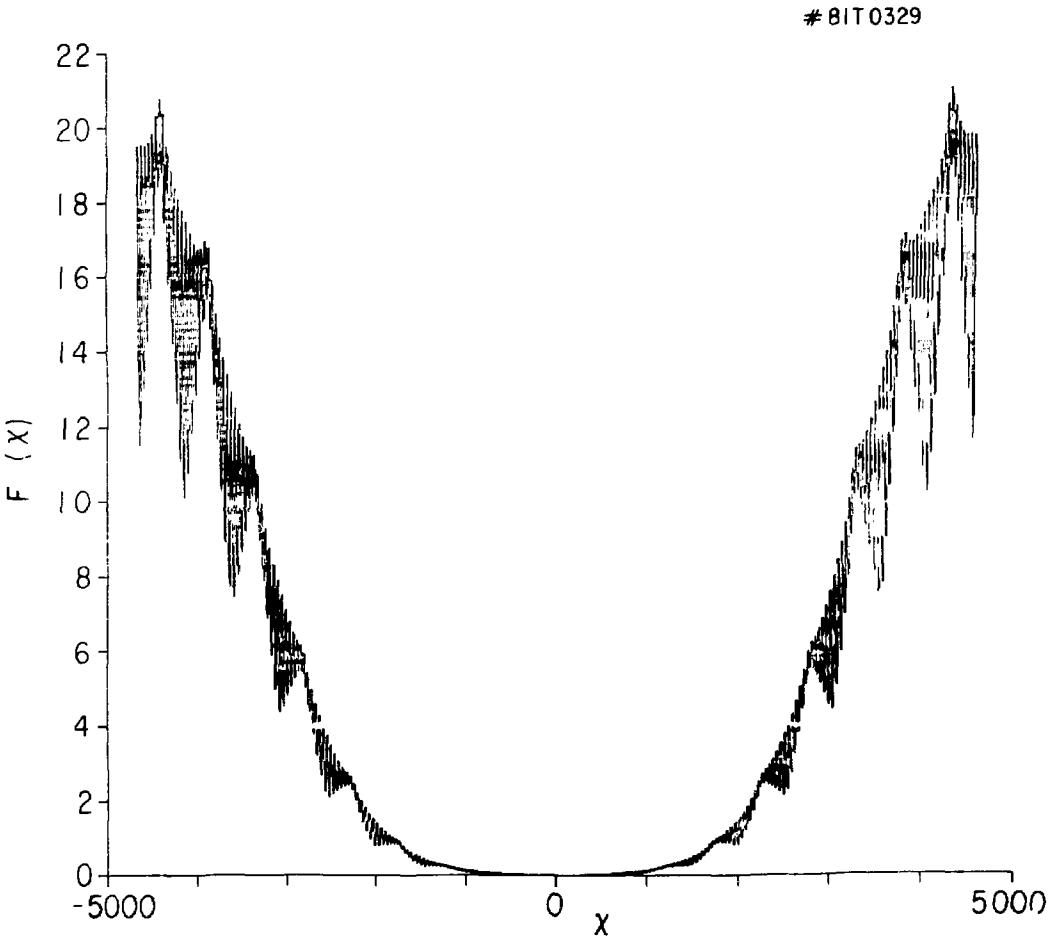

Fig. 7

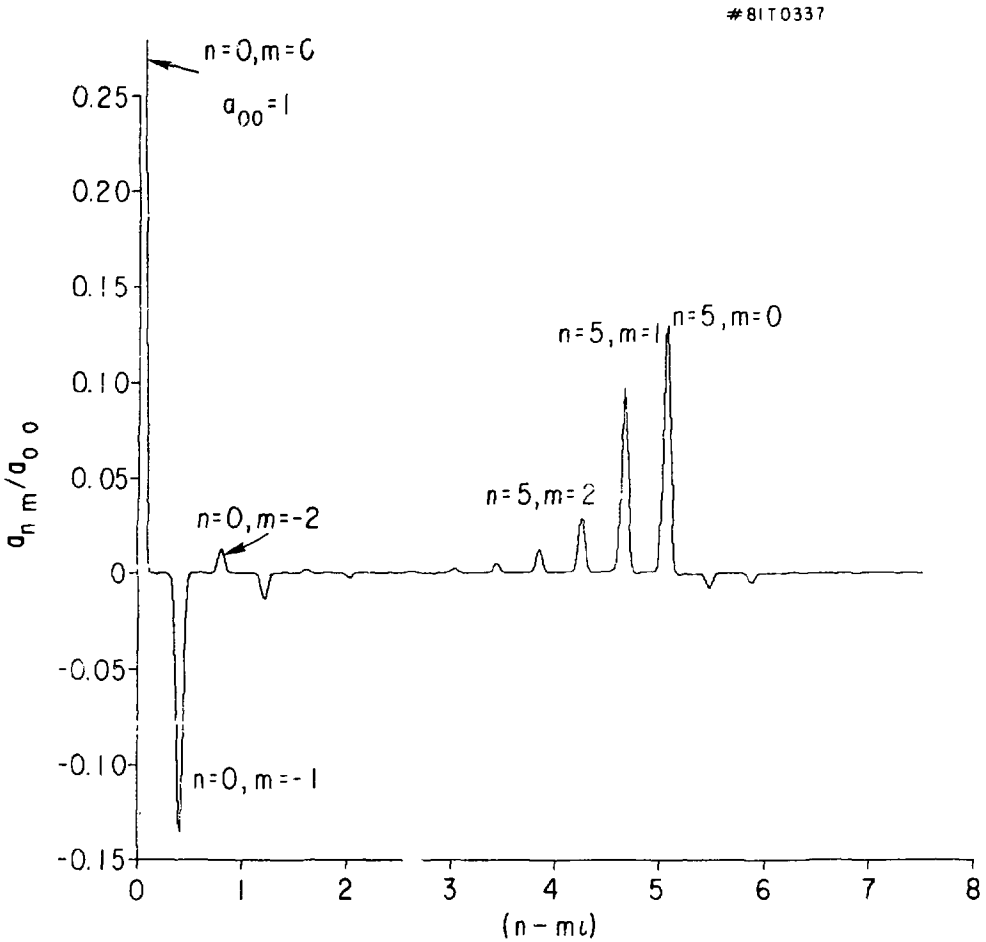
#81T0337
n=0,m=0
$a_{00}=1$
n=5,m=1
n=5,m=0
n=5,m=2
n=0,m=-2
n=0,m=-1
$a_{n\,m}/a_{0\,0}$
0.25
0.20
0.15
0.10
0.05
0
-0.05
-0.10
-0.15
0
1
2
3
4
5
6
7
8
(n-mι)

Fig. 8

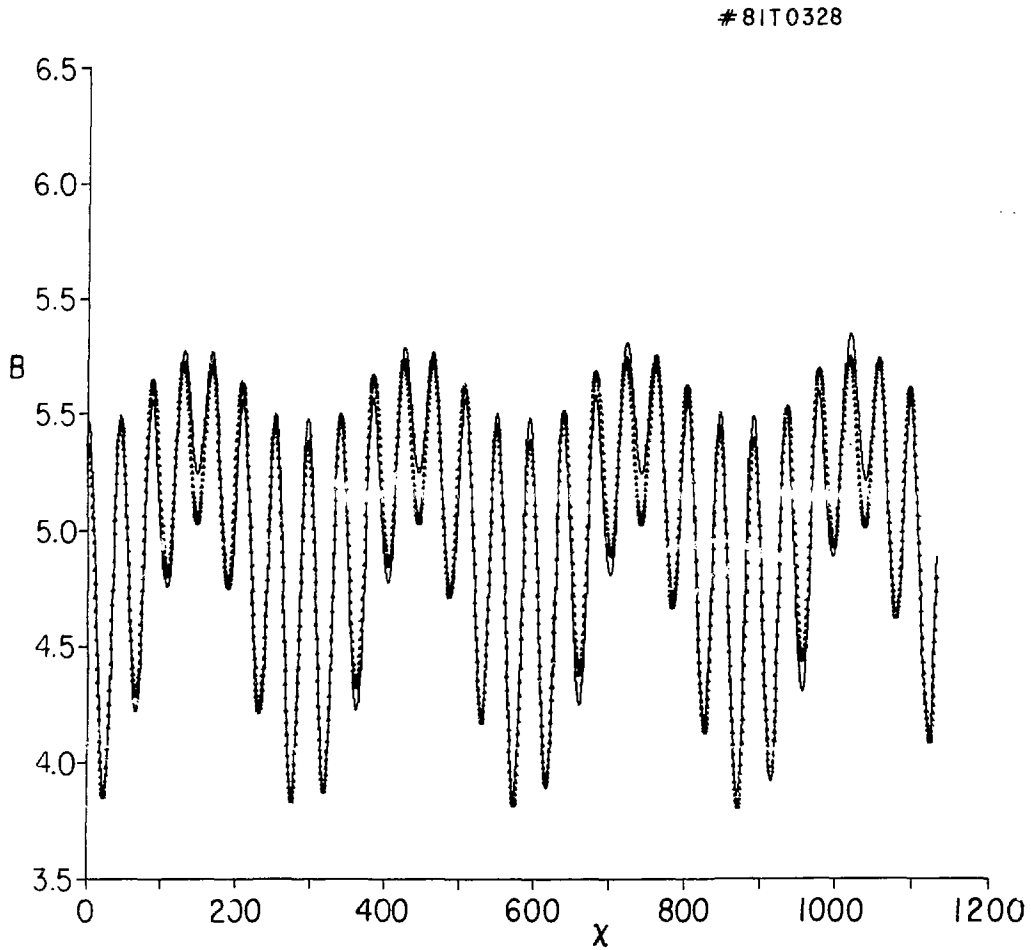

Fig. 9

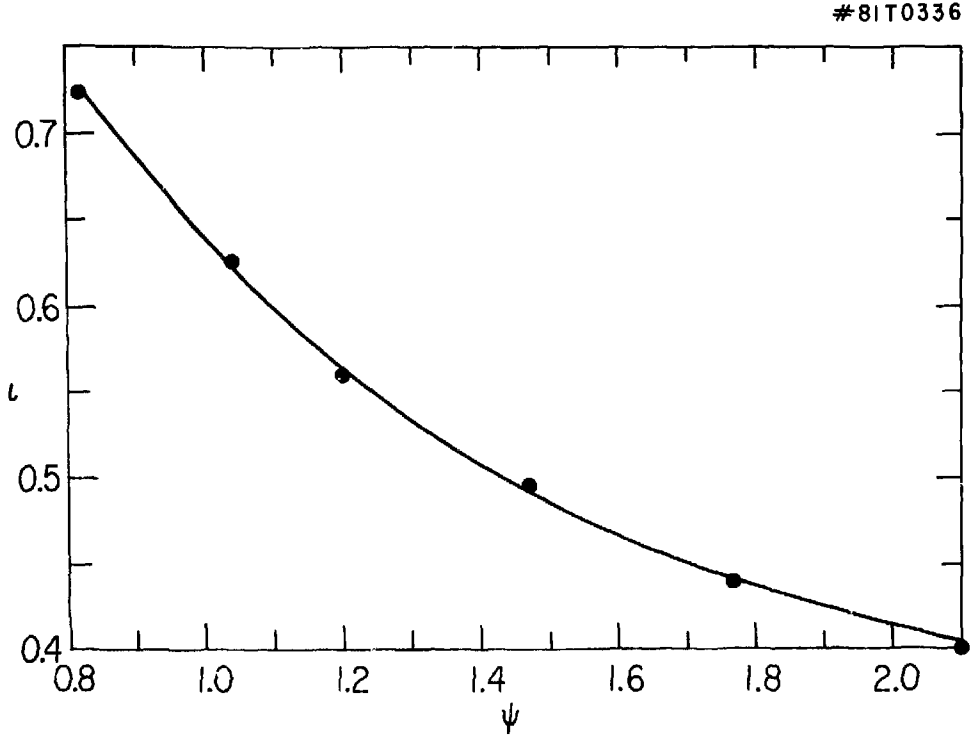

Fig. 10

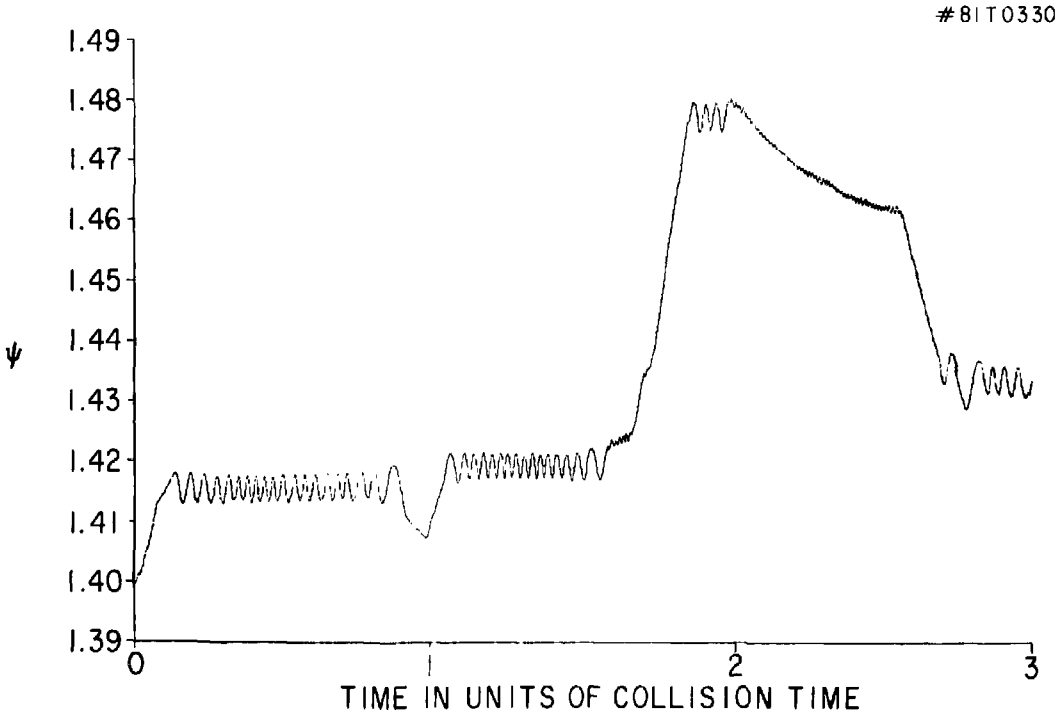
#81T0330
1.49
1.48
1.47
1.46
1.45
1.44
1.43
1.42
1.41
1.40
1.39
ψ
0
1
2
3
TIME IN UNITS OF COLLISION TIME

Fig. 11a

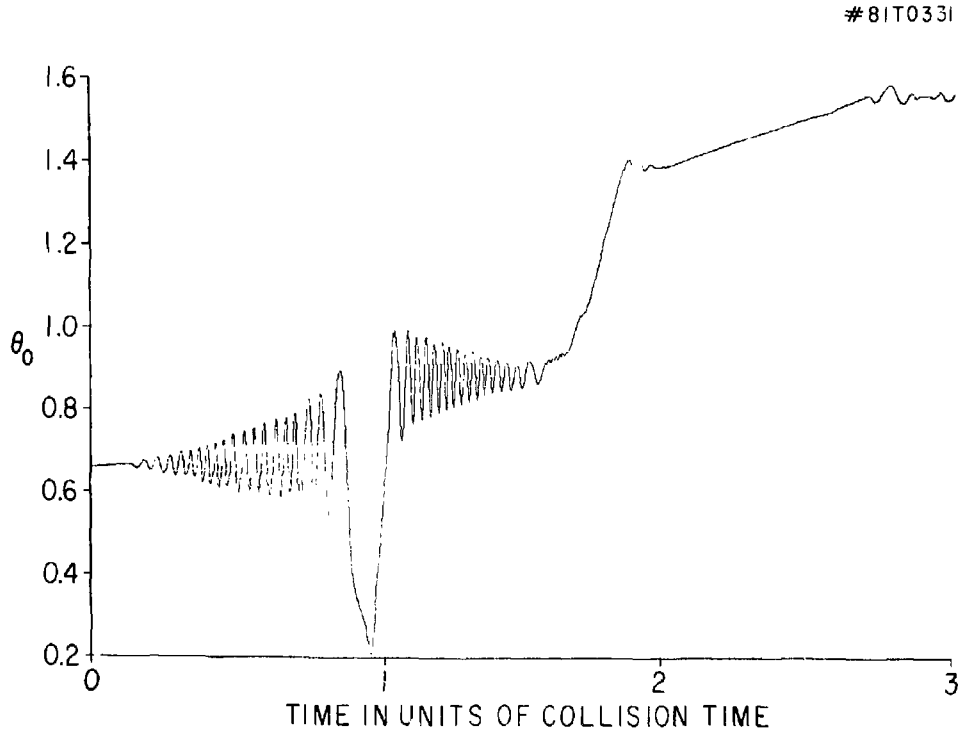
#81T0331
1.6
1.4
1.2
1.0
0.8
0.6
0.4
0.2
θ_0
0
1
2
3
TIME IN UNITS OF COLLISION TIME

Fig. 11b

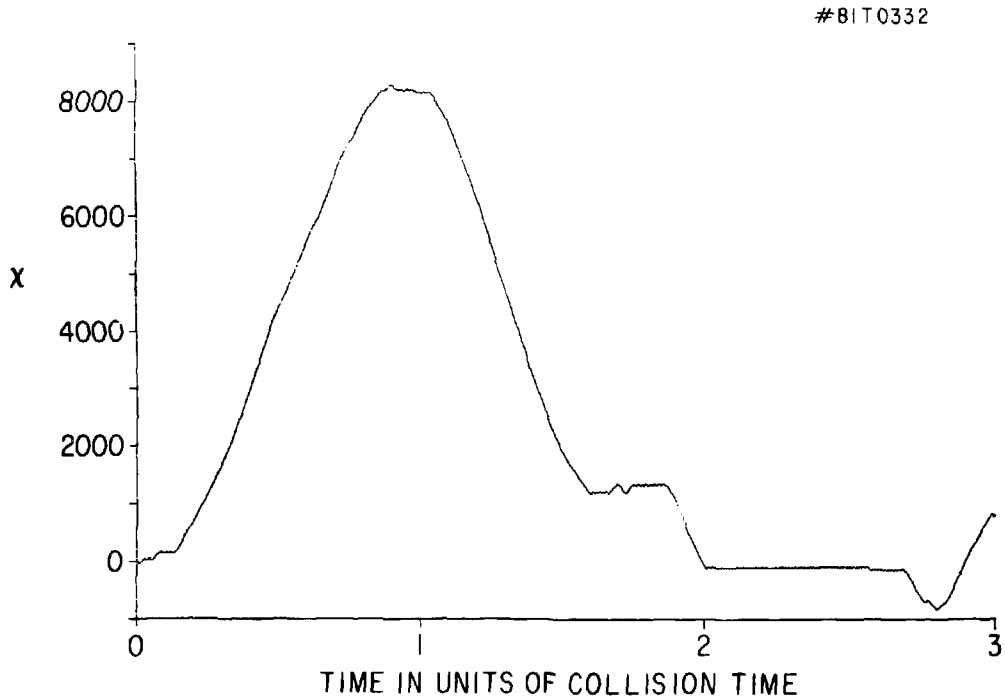
#81T0332
8000
6000
4000
2000
0
X
0
1
2
3
TIME IN UNITS OF COLLISION TIME

Fig. 11c